journal homepage: www.intl.elsevierhealth.com/journals/cmpb

Physiological modeling of tumor-affected renal circulation

Johanne Bézy-Wendling[a,b,*], *Marek Kretowski*[c]

[a] *INSERM, U642, Rennes F35000, France*
[b] *University of Rennes 1, LTSI F-35000, France*
[c] *Faculty of Computer Science, Bialystok Technical University, Wiejska 45a, 15-351 Bialystok, Poland*

ARTICLE INFO

Article history:
Received 27 April 2007
Received in revised form
25 January 2008
Accepted 28 January 2008

Keywords:
Computer modeling
Kidney
Vessels
Renal cell carcinoma
Computed tomography

ABSTRACT

One way of gaining insight into what can be observed in medical images is through physiological modeling. For instance, anatomical and functional modifications occur in the organ during the appearance and the growth of a tumor. Some of these changes concern the vascularization. We propose a computational model of tumor-affected renal circulation that represents the local heterogeneity of different parts of the kidney (cortex, medulla). We present a simulation of vascular modifications related to vessel structure, geometry, density, and blood flow in case of renal cell carcinoma. We also use our model to simulate computed tomography scans of a kidney affected by the renal cell carcinoma, at two acquisition times after injection of a contrast product. This framework, based on a physiological model of the organ and physical model of medical image acquisition, offers an opportunity to help radiologists in their diagnostic tasks. This includes the possibility of linking image descriptors with physiological perturbations and markers of pathological processes.

1. Introduction

Kidneys are vital organs that filter blood, remove waste products from the organism, and by this, maintain homeostasis [1]. They return essential substances to the blood stream while excreting toxins and metabolic wastes into the urine. As the main function of kidney is to purify blood and to equilibrate its composition, this organ is endowed with a dense network of blood vessels. Renal pathologies, whether they affect the kidney vascular network directly or indirectly, can disturb its normal functioning. Studying the renal vascular system and its macro- and microscopic, geometrical, or functional perturbations is important in understanding and eventually detecting and characterizing renal pathologies. Developing physiological models helps to understand complex in-depth phenomena underlying the observations and particularly clinical images [2].

The anatomy of renal vessels has largely been explored by means of silicon casts at the macroscopic [3–5] and microscopic [6] levels. A method of microscopic vessel analysis from images was proposed in Ref. [7], leading to topological and geometrical characterization of glomerular capillaries. More recently, Nordsletten et al. proposed a method to extract structural characteristics of the renal vasculature from microcomputer tomography images [8] of the rat. These *in vitro* and *in vivo* studies provide purely geometrical and structural vascular features and, moreover, they necessitate collecting important quantities of data, to reproduce inter-patients variability or various pathological modifications. In Ref. [9], Zamir has shown the possibility to reproduce fractal trees with properties similar to vascular trees (angles, lengths, and calibers), using the simple formalism of L-systems. One limit of this model is that it fails to mimic the heterogeneity of natural vascular trees, resulting from constraints related to organ

* *Corresponding author at*: LTSI, Université de Rennes 1, Bâtiment 22, Campus de Beaulieu, 35042 Rennes Cedex, France. Tel.: +33 2 23235604; fax: +33 2 23236917.
E-mail address: johanne.bezy@univ-rennes1.fr (J. Bézy-Wendling).
0169-2607/$ – see front matter © 2008 Elsevier Ireland Ltd. All rights reserved.
doi:10.1016/j.cmpb.2008.01.009

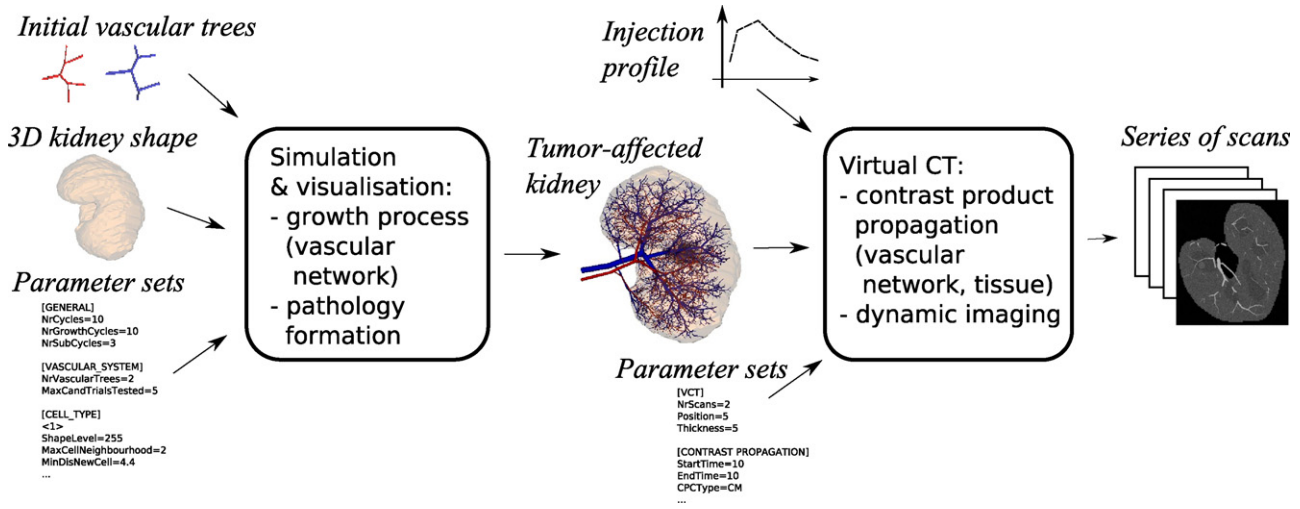

Fig. 1 – Modeling framework proposed to find relation between medical images (CT scans for instance) and vascular modifications of the kidney anatomy and physiology. The simulator consists of two main parts: the first part generates the organ and its vessels with an eventual pathology like hypervascular tumor. The second part uses this 3D simulated organ to synthetize virtual CT scans after injection of a contrast product.

anatomy and function. Other models have been proposed to reproduce the growth of three-dimensional (3D) vascular trees (and applied to the coronary arteries), for instance, the CCO model presented in Ref. [10]. These approaches, however, are suitable for the simulation of one unique tree, and do not allow the propagation of contrast agent necessary to simulate image acquisition.

Another kind of mathematical models aims at the understanding of kidney function. A well-documented survey of these models concerning glomerular filtration, tubular transport, and urinary concentrating mechanisms can be found in Ref. [11]. In Ref. [12], Hervy and Thomas propose to study the possibility that inner medullary lactate production may intervene in the urine concentrating mechanism. Their multinephron model includes vasa recta, Henle loops, and collecting ducts. Development of this kind of functional model of solute and electrolytes exchanges is also one of the objectives of the kidney part of the Physiome project [13,14].

The study that we present in this paper aims at modeling vascular heterogeneity in the kidney, and especially vascular modifications appearing with tumor development. Our goal is also to use our 3D model of tumoral vascularization to simulate clinical images of renal tumors as summarized in Fig. 1. After having simulated the growth of a normal organ, a tumor is introduced (by means of tumoral Macroscopic Functional Units (MFUs)) and then the dynamic CT image acquisition is also reproduced after simulation of the injection of a contrast agent into the main artery.

The physiological model proposed here derives from our previous work on modeling of parenchymous organs in which vascularization plays a crucial role [15,16]. For instance, we simulated the complex hepatic vascular system that consists of three trees, in both, normal and pathological cases [17].

In this work, we extend the previous model and adapt it to the complete renal vascular network, down to the arteriole and veinule level (i.e. the model treats all vessels with diameter $\geq 100\,\mu m$). The topological, geometrical, and perfusion variability is guaranteed by introducing anatomical constraints as well as perfusion properties. These features are related to the renal vascularization and its natural regional variations. Thus, the model allows us to distinguish the main renal structures where vessels are present (cortex, medulla), and to attribute adapted vascular properties to them (vascular density, perfusion). The connection between arterial and venous trees is not purely geometrical: it is suited for transfer of any substance (blood/contrast material) from one tree to the other, taking into account local haemodynamic properties (pressure, flow). We apply our model to the simulation of the main renal malignant tumor (renal cellular carcinoma), whose vascular related manifestations consist mainly in a localized hypervascularization. We illustrate geometrical modifications of the vascular network (caliber, vessels density) resulting from the tumor growth. We also depict preliminary results of simulated computed tomography (CT) scans of a kidney affected by a renal cell carcinoma (RCC). These allow us to envisage the extraction of tumoral markers from clinical images after a first step of relating image parameters to physiological properties.

This paper is organized as follows. In Section 2, we present the model of renal circulation with the description of its two main components: tissues and vessels. Section 3 is devoted to the simulation results, in the normal case of coupled growing arterial and venous trees, and in the pathological situation of RCC. Simulation results are qualitatively and quantitatively compared to real data. Finally, we discuss these results in Section 4, where we also propose future work.

2. Model of the renal circulation

As for all biological structures [18], the anatomy of the renal vascular system is the result of a long growth process. Mod-

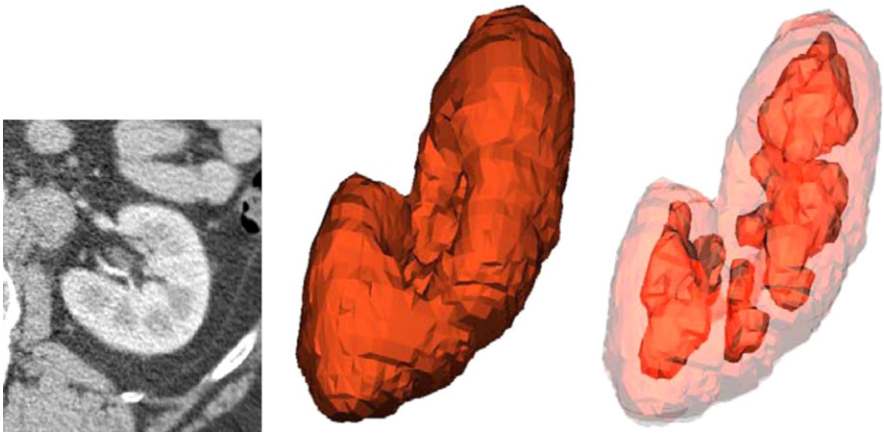

Fig. 2 – Anatomical structures used in the kidney simulation. *Left*: a cropped image (slice) of the original CT database. *Middle*: the kidney shape (result of manual segmentation of the database). *Right*: pyramids of the medulla also obtained by manual segmentation.

eling of this process is necessary to reproduce structural and geometrical characteristics of vascularization. In our model, the growth of the vascular system takes place in a three-dimensional envelope consisting of the main anatomical renal structures. Anatomical and physiological changes occur at discrete time. During each cycle, the vascular network develops by enlargement of existing vessels and sprouting of new ones, in response to increased blood perfusion, due to organ growth.

2.1. *Renal anatomical model*

In the model, the kidney is represented by a three-dimensional shape representing two kinds of tissues, cortex and medulla, whose vascularizations present several differences. Images from a three-dimensional computed tomography database were manually segmented to obtain 3D geometrical constraints on these two kinds of anatomical structures. We show one slice of the original database and the subsequent segmentation results in Fig. 2. From this adult segmented kidney, scaling is applied with different scaling factors to build a set of shapes, with increasing sizes, in order to simulate the growth of the organ.

In order to reproduce a biological tissue which is a set of identical cells, our tissue model is based on the gathering of Macroscopic Functional Units: a MFU corresponds to a small region of tissue (discretization of the organ), whose size is a parameter of the model (typically, this size is a few mm^3). Each tissue corresponds to a particular class of MFUs, with its own characteristics: rhythm of MFU division and disappearance, local density of MFUs, perfusion, blood pressure, etc.

In living organisms, cells die after a certain number of divisions (programmed cell death): at any moment, some cells are dividing and some are dying. This process is simulated by means of two coefficients: the "MFU mitosis" and "MFU necrosis" probabilities (Pb_m and Pb_n), whose temporal evolution follows exponentially decreasing profiles. These laws

$$Pb_m(t) = m_1\, e^{(-t/m_2)} \tag{1}$$

and

$$Pb_n(t) = n_1\, e^{(-t/n_2)} \tag{2}$$

assure faster rates of division and death at the beginning of the organ growth than at the adult stage [15] if the m_1, m_2, n_1, and n_2 coefficients are correctly chosen.

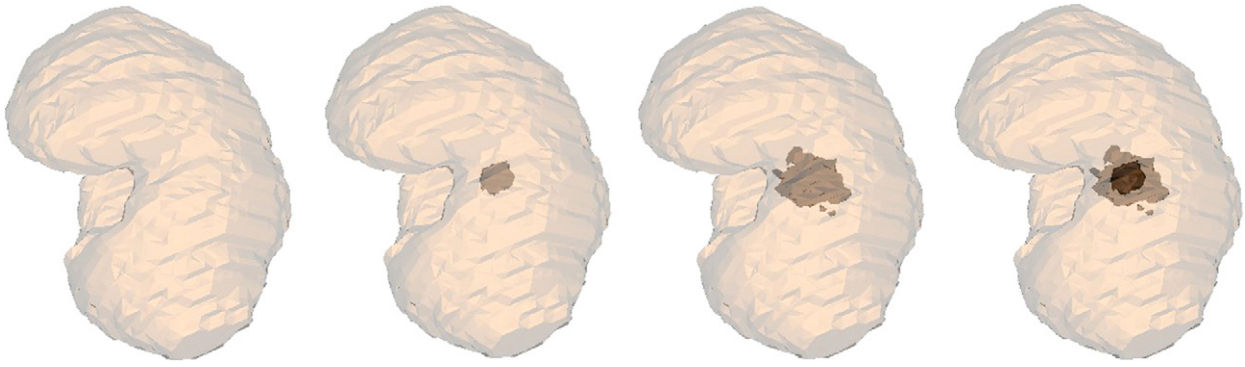

Fig. 3 – Illustration of the conversion process included in the simulator: a tumor evolution can be reproduced by means of progressive changes of tissue (and consequently vessels) properties. Here, the appearance and development of a tumor is displayed, with necrosis in its center at the end of its growth.

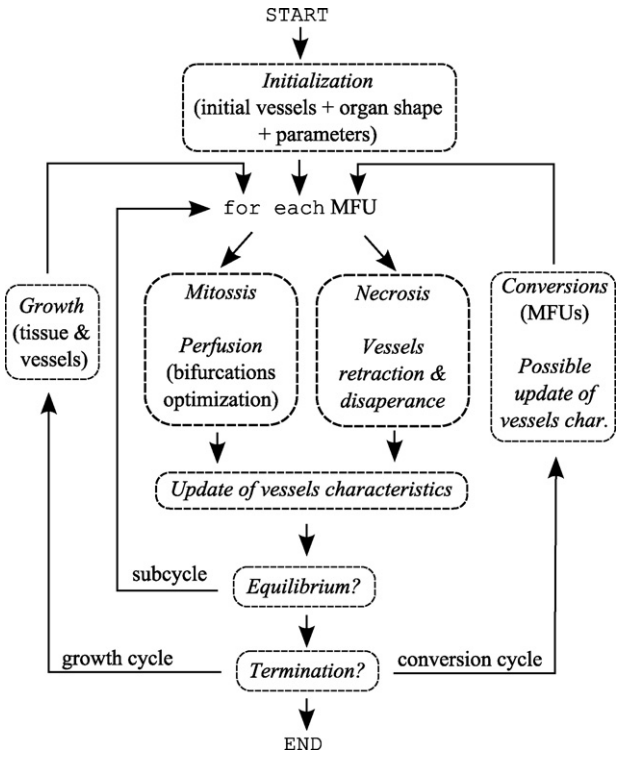

Fig. 4 – Mains steps of the development of the kidney and its vascular network, from the initialization to the end of growth.

In order to simulate different stages of pathological processes, the possibility of generating very progressive tissular modifications is introduced, by assigning temporarily changing properties to a class of MFUs. This mechanism is based on a *sequence* of *conversions*: a conversion is a time period during which a class of MFU can be changed into another class. Parallel conversion sequences can be used to simulate the evolution of one or several lesions (Fig. 3): a first lesion can appear with time changing properties, followed by the outbreak of a second local perturbation (like a necrosis in the middle of the tumor illustrated in Fig. 3). This procedure is designed to simulate evolving pathological manifestations, the progression or regression of a disease (see Section 3), or the development of metastases in the case of a tumor.

2.2. Model of vascular network

The main steps of the vascular network development are represented in Fig. 4.

2.2.1. Initialization

The kidney circulation simulation begins by the phase of model initialization where a few vessels are manually placed in the smallest 3D renal shape (about 5% of the volume of an adult kidney). After the kidney growth, these vessels generally become the main arterial and venous branches. Their position is carefully chosen in such a way that they correspond to interlobular arteries and veins. The more common case, where only one main renal artery irrigates the organ (and not the particular case where there are two renal arteries [19]), is considered.

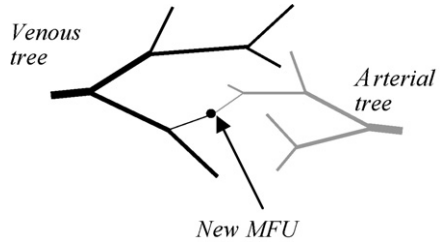

Fig. 5 – Connection of a new MFU to existing arteries and veins. Two new vessels sprout, one for each tree.

2.2.2. Development

The appearance and development of new vessels are analogous to the natural angiogenesis process: during organ growth, arterial and venous vascular trees develop simultaneously to perfuse new MFUs which are not yet irrigated because they just appeared during the growth cycle. The appearance of these new MFUs leads to the sprouting of new vessels. When a new vessel sprouts, two bifurcations are created in the vascular network: one to irrigate the MFU, coming from the arterial tree, and the second to drain it, connected to the venous tree (Fig. 5). These vessels are represented by rigid tubes, whose wall thickness depends on their type (artery or vein) and is proportional to their radius (arteries are thicker than veins). During the simulation of organ growth, vessel diameters globally increase in two possible ways. First, each time a new small vessel is added to the tree, all the haemodynamic and geometric properties of the existing vessels are re-computed taking into account the presence of this new vessel (for instance the blood flow of all the vessels up to the main one are updated, as well as their caliber). The second way consists of an artificial enlargement, applied periodically, when the organ size is increased to simulate its natural growth. The whole set of branches and bifurcations constitutes a binary tree. Fig. 6 shows the main features associated with a tree. They are essentially blood pressure and flow, and geometric parameters such as length and radius.

Each MFU is perfused by two vessels (arterial/venous), whose calibers depend on the size of the MFU, corresponding to the spatial territory irrigated by these vessels. Blood circulates from the renal arterial tree to the venous one, through MFUs. The haemodynamic problem of blood flow through vascular trees is simplified by using Poiseuille's law

$$\Delta P = Q\frac{8\mu l}{\pi r^4} \tag{3}$$

which describes the relation between blood flow (Q), pressure drop (ΔP), and blood viscosity (μ) in a cylindrical tube with a given geometry (radius r, length l). Rigorously, this law is verified only for laminar flows, in which the viscosity is constant. This is the case for blood in vessels whose radius is larger than 0.1 mm. For smaller vessels, the viscosity depends on several parameters such as the vessel caliber, the density of red blood cells, etc. The fact that it is used for all the vessels of the model

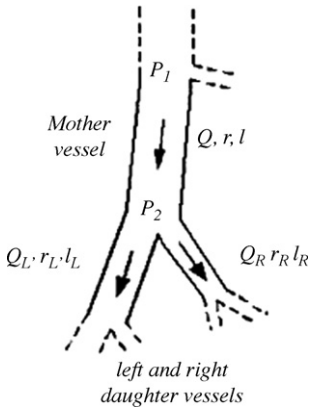

Fig. 6 – Successive bifurcations constituting the binary vascular tree. Features P, Q, r, and l correspond to blood pressure, blood flow, radius and length associated with the mother and daughter vessels. The angle between the two daughter vessels is variable, and is the result of a local optimization process of the bifurcation based on the criteria of minimum volume.

constitutes one of the simplifications of our model. Local flow also obeys the law of conversation of matter

$$Q_F = Q_{SR} + Q_{SL} \quad (4)$$

(blood flow in the father vessel Q_F is the sum of the blood flows of the right and left sons Q_{SR}, Q_{SL}), and the bifurcation law relating the vessel radii

$$r^\gamma = r_L^\gamma + r_R^\gamma \quad (5)$$

Geometry of the vessels resulting from a new bifurcation is optimized, considering a few neighboring vessels and choosing the configuration that necessitates the smallest addition to the blood volume [20,21]. Moreover, potential contacts between vessels are avoided by testing whether the new bifurcations lead to collisions between vessels of the same tree or of distinct trees. The method we propose for the selection of the minimal volume, non-intersecting configuration of vessels, for the perfusion of a new MFU is described in detail in Ref. [17]. When a new vessel appears to perfuse a new MFU, its geometric (caliber) and haemodynamic (pressure, flow) characteristics depend on which class of MFUs (for example, normal class or pathological class) it belongs to.

The vessel characteristics then evolve during the whole growth simulation, according to connections with other vessels and local and global vascular modifications (for instance, blood flow of normal vessels will change if a tumor develops in their neighbourhood). Each tree is maintained consistent throughout its growth, which means that the three aforementioned physical laws are verified, as well as the predefined pressure at the tree entrance and at the tree extremities, especially when new vessels are added to an existing tree. The method used to maintain the consistency of a bifurcation is presented in Ref. [22], and its extension to a whole tree is also detailed.

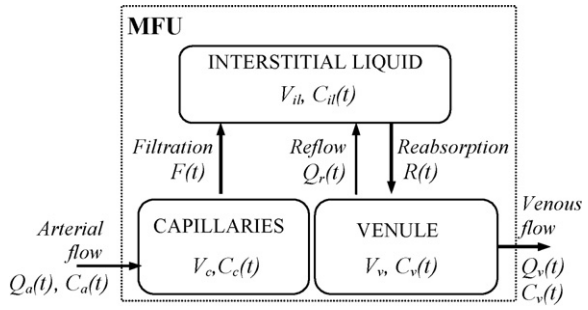

Fig. 7 – The microscopic compartment model used to simulate the propagation of blood and contrast product, from the arterial to the venous tree.

In some cases, vessels can also disappear, when the blood needs of the perfused tissue are decreasing. In this situation, the geometric and haemodynamic properties of the local vascular system (the two bifurcations of the two trees) are first modified, and these changes also affect the global vascular network, in such a way that the consistency is still maintained.

2.2.3. *Microscopic model of vascular/extravascular exchanges*

In the macroscopic model of arterial and venous renal vascularization, blood goes from the arterial tree to the venous tree through the MFUs. Each MFU is represented by a microscopic model based on compartments displayed in Fig. 7. The compartmental model allows us to compute blood flow as well as the propagation of contrast product in vessels that are smaller than those represented in the macroscopic model (arterioles, venules). It is mainly used to compute the amount of contrast dye, in order to correctly simulate the acquisition of dynamic CT scan acquisition (see Section 3.2). In this model, blood (and contrast product if some has been injected) flows from the arteriole to the capillaries, then it enters the interstitial liquid compartment and leaves the MFU via the venule. This model is a simplified version of the model that we proposed to simulate the hepatic microvascularization in [23]. The main difference

Table 1 – Parameters used to simulate the renal circulation

Pressure in renal artery	95 mmHg
Pressure in efferent arterioles and venules	10–15 mmHg
Pressure in renal vein	5 mmHg
Blood flow at MFU level—normal	0.156 ml/min
Blood flow at MFU level—hypervascular tumor	0.780 ml/min
Blood flow at MFU level—necrotic part	0 ml/min
Number of growth cycles	100
Volume growth	1–400 cm^3
Number of MFUs in normal kidney	~3200
Wall thickness ratio (fraction of vessel radius)—arteries	0.2
Wall thickness ratio (fraction of vessel radius)—veins	0.1
Gamma (bifurcation law)	2.7
Blood viscosity	0.0036 Pa s

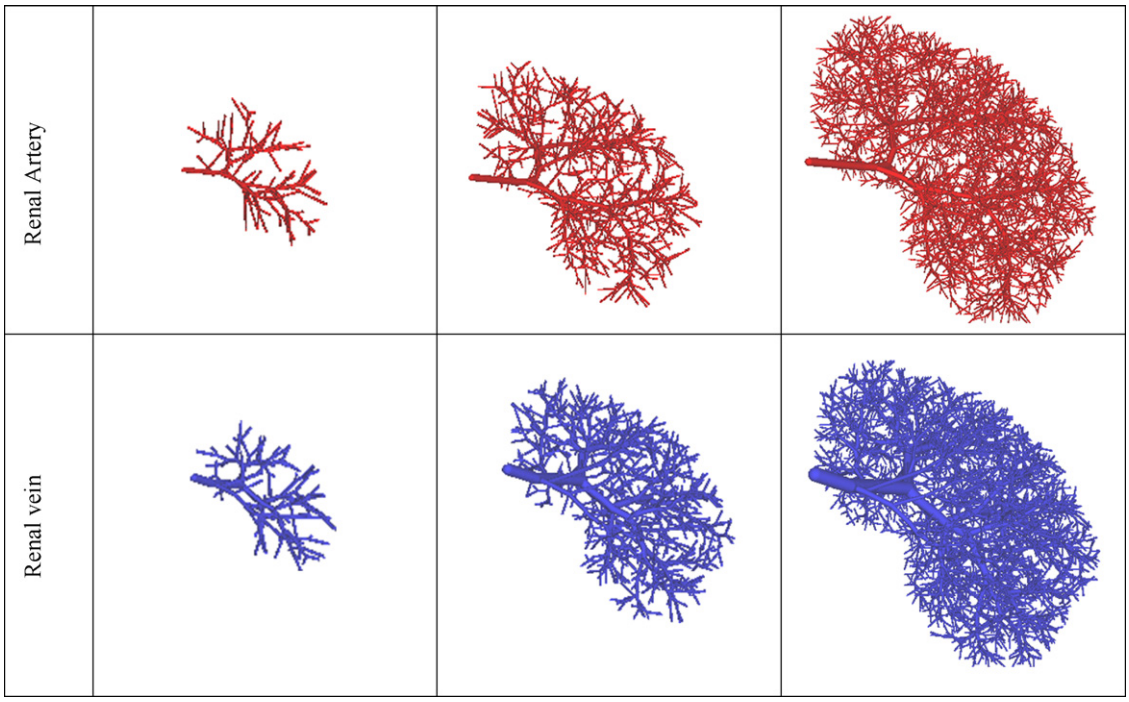

Fig. 8 – Simulation results representing the growth of arterial and venous renal trees, in normal situation.

is that in the case of the kidney, only one input is considered. The propagation of contrast agent is described by the system of differential equations

$$V_C \frac{dC_C(t)}{dt} = C_a(t)Q_a(t) + C_v(t)Q_v(t) - C_C(t)F(t) \quad (6)$$

$$V_{il} \frac{dC_{il}(t)}{dt} = C_c(t)F(t) + C_v(t)Q_r(t) - C_{il}(t)R(t) \quad (7)$$

$$V_v \frac{dC_v(t)}{dt} = C_{il}(t)R(t) - C_v(t)(Q_r(t) - Q_v(t)) \quad (8)$$

where the variation of molecular concentration $C(t)$ in each compartment is computed as a function of time. The sub-

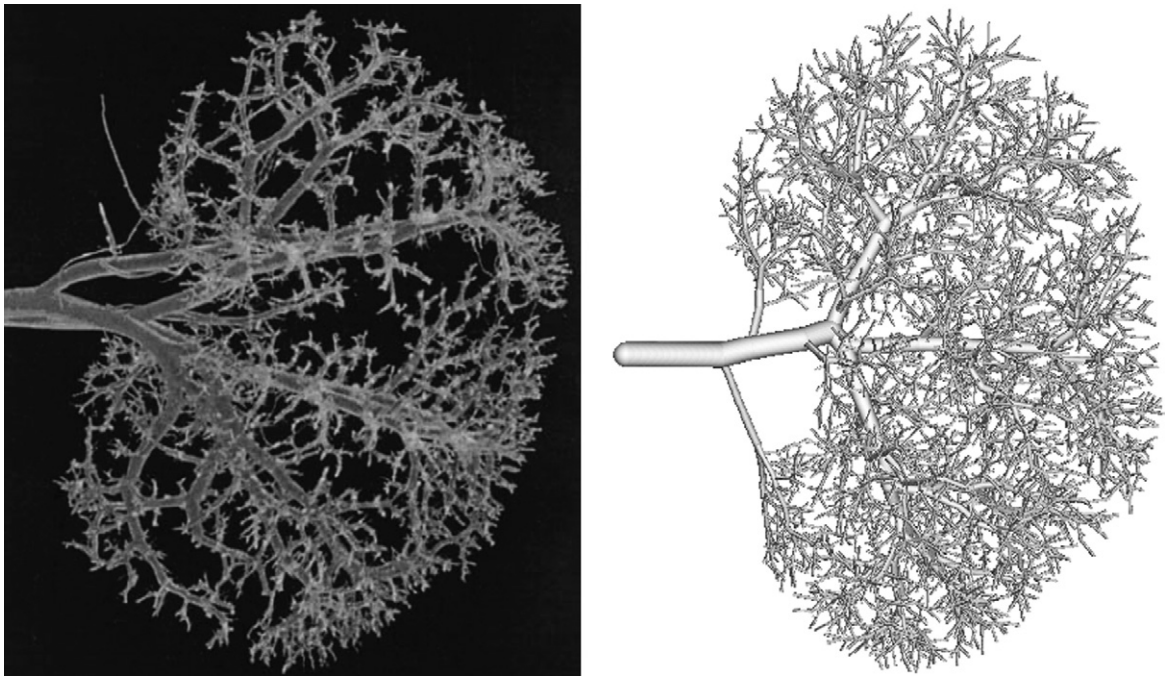

Fig. 9 – Comparison between simulated and real renal vascular network. *Left*: silicon cast of a renal vein of a rat (due to Zamir [9]). *Right*: simulated renal vein, obtained by means of the proposed model of renal circulation, using parameters of Table 1.

scripts correspond to the initial of each compartment (a, c, il and v, stand for arteriole, capillaries, interstitial liquid and venule, respectively). The compartment volumes (V_c, V_{il} and V_v) are obtained by dividing the corresponding volumes (capillaries, interstitial liquid and vein) of the kidney by the total number of MFUs. F, R and Q_r are the transvascular flows. Q_a and Q_v are the arterial and venous flow at the entry and output of the MFU. Knowing the contrast agent concentration in each compartment allows us to compute the total concentration in each MFU, which is necessary for the simulation of dynamic CT scans.

2.3. *CT scan modeling*

The first step to simulate dynamic CT is injection of contrast medium in the renal artery. It propagates through vessels and tissue. The contrast concentration is calculated in all the macroscopic vessels (all of whose geometrical and haemody-

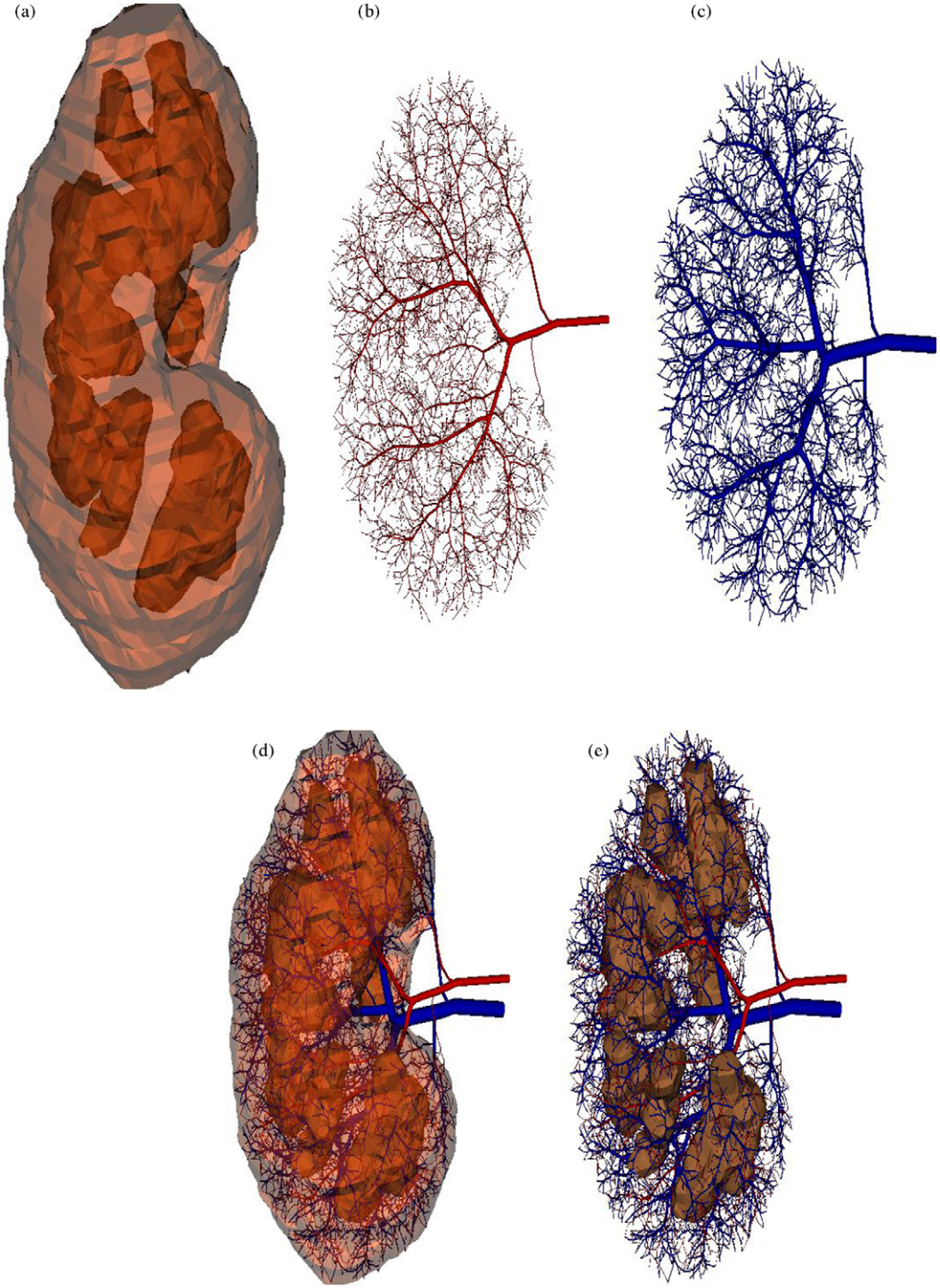

Fig. 10 – Simulation results of kidney vascularization (artery in red, vein in blue): (a) 3D envelopes of the cortex and medullar pyramids, (b) renal artery, (c) renal vein, (d) and (e) the two coupled trees.

namic characteristics are known, thus allowing calculation of the transit time of the contrast product from the main artery to each vessel of the tree), as well as in each MFU (with the compartmental approach presented before). Each voxel is assigned an attenuation coefficient that depends on its composition (blood/tissue/contrast medium concentration) [17]. Then, the CT scan acquisition is carried out through the classical back-projection algorithm: X-ray parallel projections with noise-added are computed, using the Radon transform, projections are filtered in the Fourier domain, by a band-limited filter and a back-projection is applied to reconstruct the image. With the simulator, the user can set some acquisition parameters such as the slice orientation, thickness, and the image resolution (pixel size).

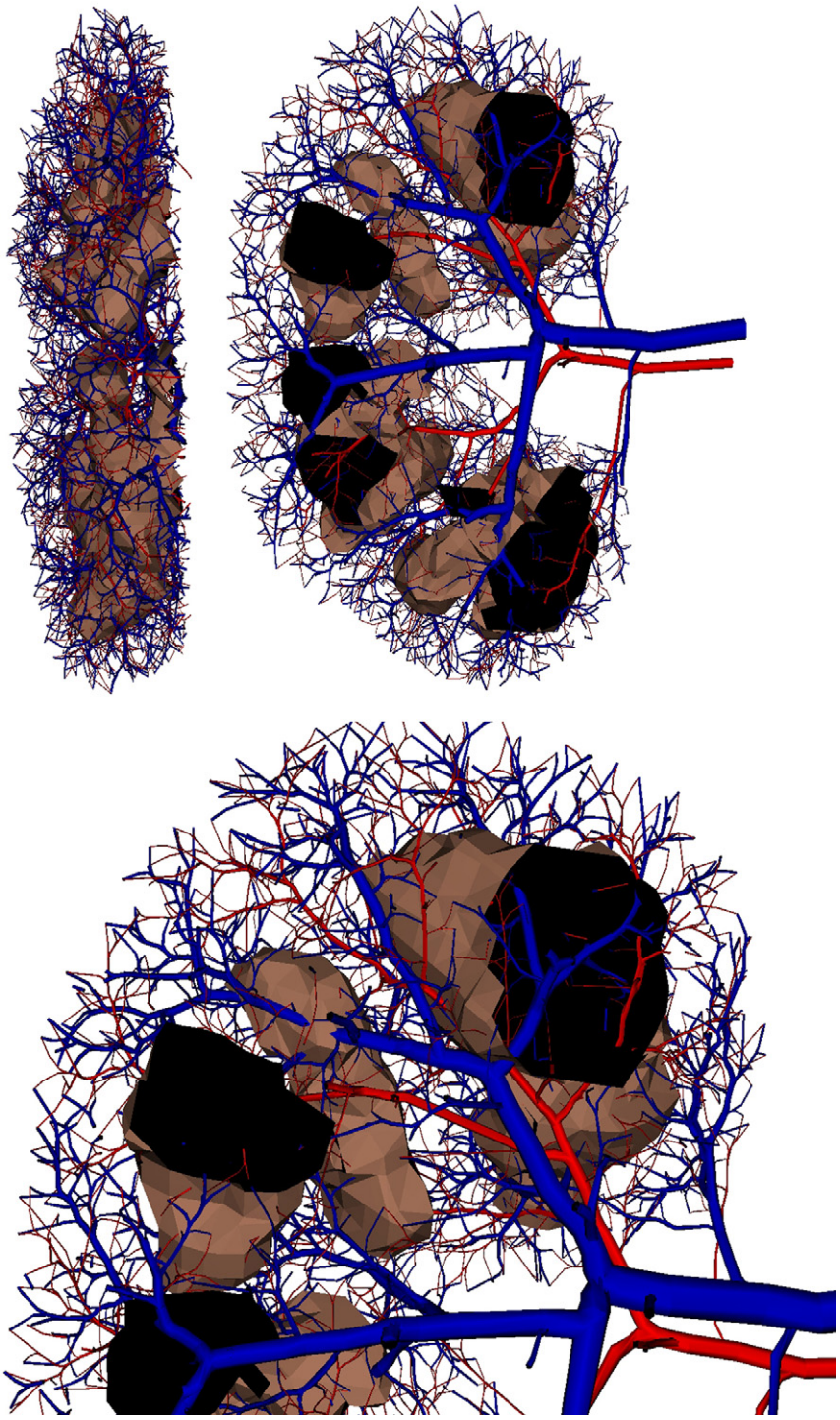

Fig. 11 – Differences between vascularization of cortex and medulla. The renal arterial and venous trees are displayed. *Left*: kidney is cut vertically to show vessels inside the organ. *Middle*: rotated kidney. *Right*: zoom of the upper part of the kidney. It can be observed than the cortex vascular network is more developed than the medulla's one.

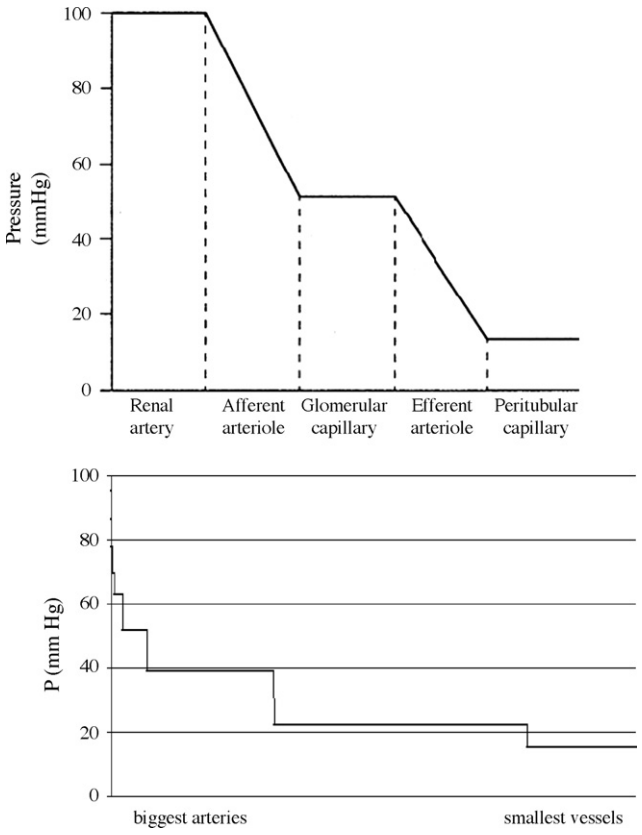

Fig. 12 – Pressure profile in the arterial vascular tree. *Top*: in vivo values found in literature [20]. *Bottom*: values coming from the simulated arterial tree: vessel radius in the *x*-axis in decreasing order. The represented pressure (horizontal lines) in the range of radii is the average of values in the range. The renal artery is represented by one point, and not a line like in the left graph.

3. Results

All the results presented in this section were obtained by means of a simulator implemented in C++. This system can be used to simulate the organ growth, the vascular trees (normal and pathological), and to render the CT images (as shown in Fig. 1). It also enables the visualization of complex 3D anatomical structures.

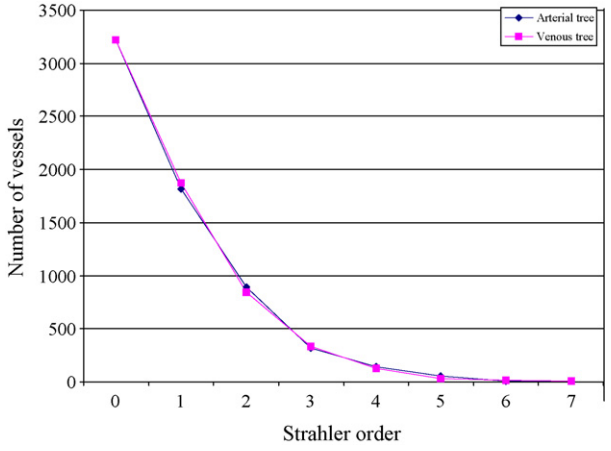

Fig. 13 – Number of vessels in the arterial and venous trees versus Strahler order.

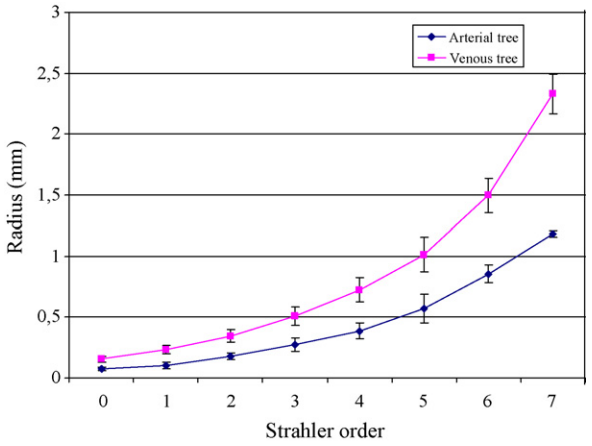

Fig. 14 – Mean radius of vessels in the simulated trees versus Strahler order.

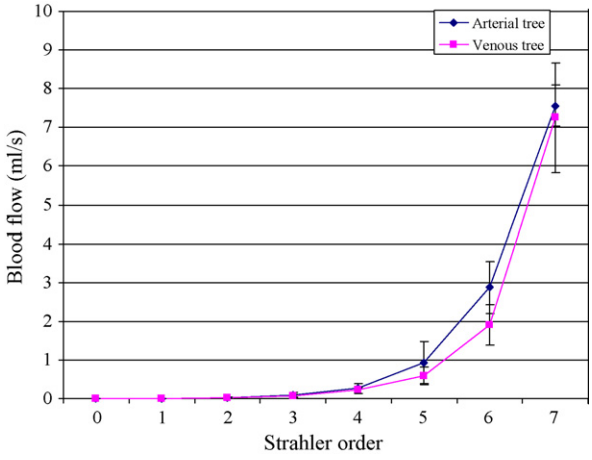

Fig. 15 – Mean blood flow in simulated arteries and veins. Strahler order is represented on the *x*-axis.

The main parameters used in the simulation of renal circulation are summarized in Table 1. They are principally pressure in the main vessels (renal artery and renal vein) and in the smallest simulated vessels (arterioles and venules), and total renal blood flow in the kidney. Other parameters depend on the type of tissue (normal/abnormal, and cortex/pyramids in medulla), for instance, the MFUs rhythm of regeneration or the local density of MFUs.

3.1. *Growth of the arterial and venous renal systems*

Fig. 8 shows images of the growth of the renal vascular system. The arterial and the venous vascular trees are presented, at three different moments of the organ growth. As the growth of the kidney is correlated with the apparition of new MFUs, it also leads to an important increase of the number of vessels at each cycle. When the simulation is finished, the vascular

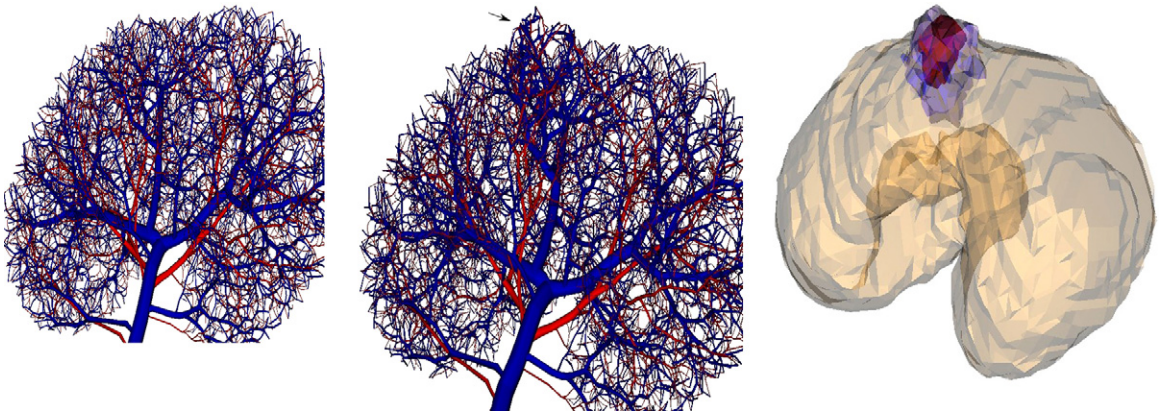

Fig. 16 – Simulation results of a renal cellular carinoma (RCC). *Left*: normal vascular trees (arteries in red and veins in blue). *Middle*: vascular trees in the organ with RCC of the left figure (rotated view). Hypervascularization is shown by the arrow. *Right*: three different tissues considered in the tumoral kidney: normal (in brown), hypervascularized (blue), and necrosis (red).

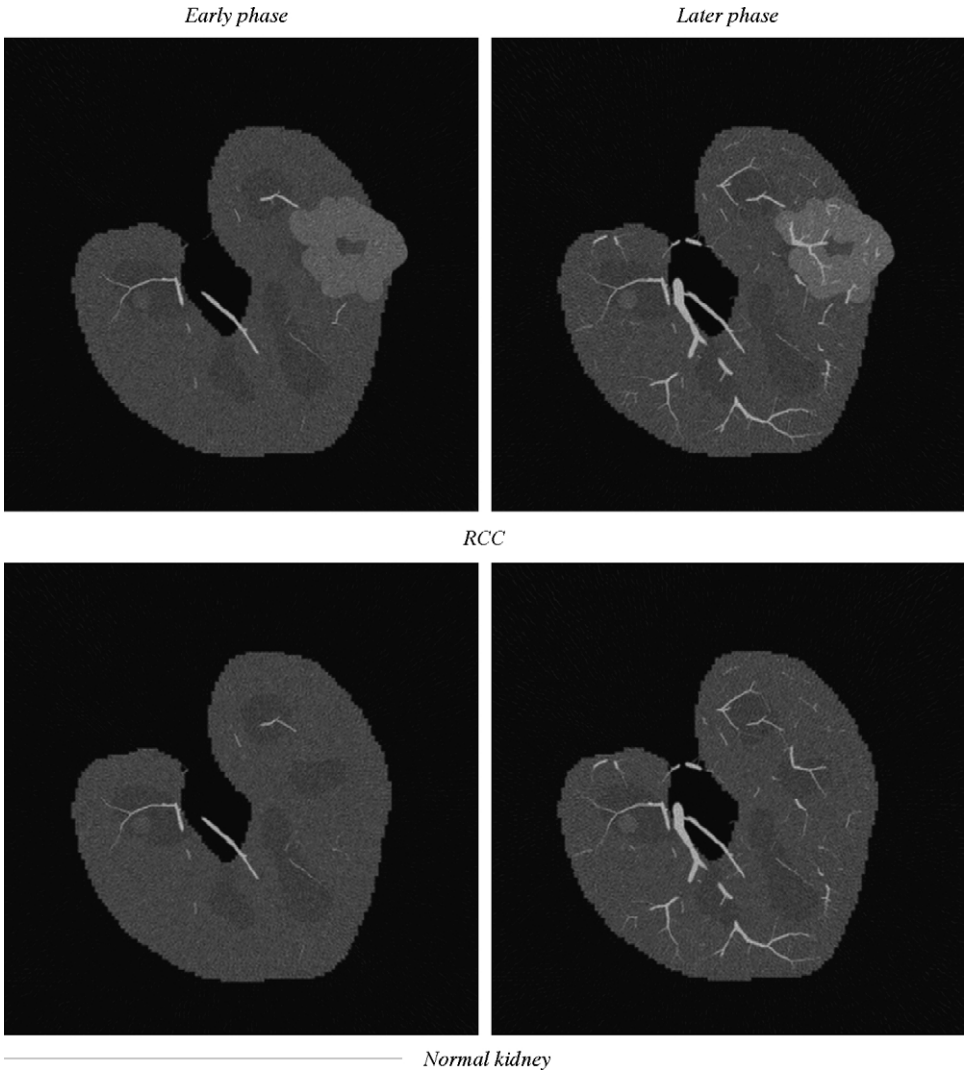

Fig. 17 – Simulated CT images of the kidney at two acquisition times during contrast product propagation.

network is made of around 6000 of vessel segments. The renal vein at the end of the simulation is represented in Fig. 9. The tree structure and the vessels geometry can be visually compared to a renal vein silicon cast (due to Zamir [9]). Even if it is only a qualitative procedure, this visual comparison shows that these two vascular trees are strongly similar, proving the potential of the proposed model to represent natural heterogen vascular structures. As we did not have access to silicon casts (except published images), we did not perform a quantitative comparison with human renal vessels.

Fig. 10 shows the simulation results of complete kidney vascularization. Fig. 11 distinguishes differences between the simulated cortical and medullar vascularization: in the model, vessels appear more numerous in the cortex than in the medulla. These differences from actual kidney vascularization can be explained by calibers of simulated vessels (superior to 100 μm), and very few vessels of this size are present in the medulla (which is mainly supplied by vasa recta, whose diameter is very small—10–20 μm). The other explanation is that in the model, the medulla is partly composed of pyramids inside which vessels are absent. Fig. 12 displays the haemodynamic characteristics of the simulated arterial network: blood pressure is represented for varying vessel diameters. We averaged the values of pressure for vessels whose radius falls within certain ranges, which led to a representation by horizontal lines instead of one point per vessel. This profile is in accordance with that of renal circulation [24]. It is also the case for the main vessel diameters. At the end of the simulated kidney growth, the diameter of the renal artery is 2.5 mm, and that of the renal vein is 5 mm. These values also correspond to characteristics of kidney vascularization.

A quantitative evaluation of the geometrical and structural characteristics of the simulated vascular trees was also realized. The first step of this evaluation was to associate an order to each vessel of the network. We used the Strahler ordering method to compute the vessel orders [25,8]. A leaf of the tree is given order 0. Then, when two vessels of order i and j are connected creating a bifurcation, their parent vessel is assigned the following order: $i+1$ if $i=j$, and $\sup(i, j)$ if $i\neq j$. Then, for the two renal vascular trees (arterial and venous), the number of vessels, the mean value of radius, length, and blood flow have been computed for each of the seven orders. Figs. 13–15 show the evolution of these vascular properties with Strahler order. Even if not compared with the same kind of data for real vascular trees of humans, it can be noticed that the evolution of the number of vessels, the radius and the blood flow seem to be coherent, with very progressive variations from the minimal to the maximal value.

3.2. *Simulation of renal cell carcinoma*

Renal cell carcinoma is the most common form of renal malignant tumor, representing 3% of adult cancers. An increasing incidence has been noticed over the last years. Early diagnosis of kidney cancer is important. Detection, anatomic extent assessment and tumor characterization can lead to an optimized choice of treatment, and, consequently, to an increased chance of survival for the patient. At a macroscopic level, the RCC is a rounded mass, often heterogeneous with hypervascularized regions as well as necrotic parts.

To simulate the growth of this kind of lesion, we introduced a new class of MFUs inside the organ, among the normal MFUs. One parameter of this second class is an abnormally high rate of cell division, characterizing natural tumoral processes. The MFUs local density is also increased compared to normal renal tissue. We used the sequence of conversions process (see Section 2.1) to make this lesion evolve, with a progressive modification of the MFUs constituting its central part: their properties (like blood flow) are gradually modified. The hypervascularization of the core of the lesion is progressively transformed into a hypovascularized tissue due to necrosis.

Fig. 16 presents the simulation of a renal cell carcinoma, which grew in the cortex. MFUs are materialized by small spheres, and the two main types of MFUs are represented at two tumor stages (totally hypervascularized, and necrosis of the central region, which is a usual natural evolution of this kind of tumor [26]). The corresponding vascular network is shown with arteries and veins, connected at each MFU. This lesion is situated in the cortex, at the organ periphery, and goes slightly over the kidney edges, as generally observed with RCC. The tumor is well visible in the CT image of Fig. 17. These CT scans simulated at two acquisition times are obtained by applying the back-projection algorithm from the simulated kidney and its vascular network.

4. Conclusion

In this paper, we present a model of renal circulation. It is a knowledge-based model including anatomical and functional properties of the renal vascular network, from the main branches down to small arteries and veins (interlobar vessels). We used this model to simulate the kidney vascular network in both normal and pathological conditions. In the first case, we show that the simulated vascularization is qualitatively close to vascularization observed in real kidneys, both in terms of their structure (bifurcation angles) and geometry (vessel radii, lengths). Quantitative measures of pressure confirm this agreement between modeled and real vascular trees, as far as haemodynamic features are concerned. Significant heterogeneity, representative of natural variability, can be observed in these characteristics. This is an expected consequence of the growth process used to generate the final network: each vascular tree is progressively modified in order to satisfy local blood needs. These blood needs evolve with time during tissue growth and cells division. General physical laws are verified throughout the network development, and geometrical constraints lead to realistic geometrical configurations. Finally, functional characteristics of the organ are at the origin of vascular variations between different kinds of tissues. This last property is illustrated by the differences between the high density of cortical vessels, compared to very few vessels in the medulla. The pathology we chose to reproduce here is the most common malignant tumor of the kidney, renal cell carcinoma. In cancer imaging, this modeling approach could be used for better understanding of the growth of renal tumors, by simulating different stages of tumor progression (avascular, vascular, necrosis).

One of the applications of this work is to use the 3D simulated kidney to synthetize dynamic images like CT or

magnetic resonance, in order to find image markers of tumoral development. Studying the effect on the lesion of therapeutical treatments like chemotherapy, radiofrequency, or high intensity focused ultrasound can also be envisaged using this kind of model, with the objective of optimizing the protocol (dosimetry, probe position).

The microscopic model, acceptable for simulation general microvascular exchanges turns out to be very simplified compared to real mechanisms that happen actually in the renal microvascularization, and will have to be ameliorated in future work.

Acknowledgments

The authors would like to thank Dr. Yan Rolland (Department of Radiology of the Rennes Hospital), and Pr. Jean-Louis Coatrieux (LTSI, INSERM, Rennes 1 University) for their stimulating discussions and inspiring comments.

REFERENCES

[1] B.M. Brenner, Brenner and Rector's: The Kidney, 7th ed., Saunders, 2003, 3072 pp.
[2] J. Demongeot, J. Bézy-Wendling, J. Mattes, P. Haigron, N. Glade, J.L. Coatrieux, Multiscale modeling and imaging: the challenges of biocomplexity, Proc. IEEE 91 (10) (2003) 1723–1737.
[3] F.J. Sampaio, A.H. Aragao, Anatomical relationship between the intrarenal arteries and the kidney collecting system, J. Urol. 143 (4) (1990) 679–681.
[4] F.J. Sampaio, Anatomical background for nephron-sparing surgery in renal cell carcinoma, J. Urol. 147 (4) (1992) 999–1005.
[5] G.S. Longia, V. Kumar, S.K. Saxena, C.D. Gupta, Surface projection of arterial segments in the human kidney, Acta Anat. (Basel) 113 (2) (1982) 145–150.
[6] G.S. Longia, V. Kumar, S. Longia, Microarterial pattern of human kidney, Anat. Anzeiger 163 (2) (1987) 129–137.
[7] L. Antiga, E. Bodgan, G. Remuzzi, A. abd Remuzzi, Automatic generation of glomerular capillary topological organization, Microvasc. Res. 62 (2001) 346–354.
[8] A. Nordsletten, S. Blackett, M.D. Bentley, E. Ritman, N.P. Smith, Structural Morphology of renal vasculature, Am. J. Physiol. Heart Circ. Physiol. 291 (2006) H296–H309.
[9] M. Zamir, Arterial branching within the confines of fractal L-system formalism, J. Gen. Physiol. 118 (3) (2001) 267–275.
[10] W. Schreiner, et al., Optimized arterial trees supplying hollow organs, Med. Eng. Phys. 28 (2006) 416–429.
[11] S.R. Thomas, A.T. Layton, H.E. Layton, L.C. Moore, Kidney modeling: Status and perspectives, Proc. IEEE 94 (4) (2006) 740–752.
[12] S. Hervy, S.R. Thomas, Inner medullary lactate production and urine-concentrating mechanism: a flat medullary model, Am. J. Physiol. Renal Physiol. 284 (2003) 65–81.
[13] http://www.physiome.org/.
[14] S.R. Thomas, F. Tahi, P. Harris, A. Lonie, The renal physiome project, Proceedings of the 3rd IEEE International Symposium on Biomedical Imaging: From Nano to Macro, Arlington, Transactions of IEEE, doi10.1109/ISBI.2006.1625044, 2006, pp. 820–823.
[15] J. Bezy-Wendling, A. Bruno, A 3D dynamic model of vascular trees, J. Biol. Syst. 7 (1) (1999) 11–31.
[16] Y. Rolland, J. Bezy-Wendling, R. Duvauferrier, A. Bruno, Modeling of the parenchymous vascularization and perfusion, Invest. Radiol. 34 (3) (1999) 171–175.
[17] M. Kretowski, Y. Rolland, J. Bézy-Wendling, J.L. Coatrieux, Physiologically based modeling for medical image analysis: application to 3D vascular networks and CT scan angiography, IEEE Trans. Med. Imaging 22 (1) (2003) 248–257.
[18] D.W. Thompson, On Growth and Form, Abridged ed., Cambridge University Press, 1961.
[19] L.D. Dworkin, B.M. Brenner, The renal circulations, in: B.M. Brenner (Ed.), Brenner and Rector's: The Kidney, Saunders, 2003.
[20] M. Zamir, Optimality principles in arterial branching, J. Theor. Biol. 62 (1976) 227–251.
[21] A. Kamiya, T. Togawa, Optimal branching structure of the vascular trees, Bull. Math. Biophys. 34 (1972) 431–438.
[22] M. Kretowski, J. Bézy-Wendling, Y. Rolland, J.L. Coatrieux, Fast 3D modeling of vascular trees, Comput. Methods Programs Biomed. 70 (2) (2003) 129–136.
[23] M. Kretowski, J. Bezy-Wendling, P. Coupe, Simulation of biphasic CT findings in hepatic cellular carcinoma by a two-level physiological model, IEEE TBME 54 (March 3) (2007) 538–542.
[24] A. Gougoux, La physiologie du rein et des liquides corporels, Boucherville, Gaetan Morin, 1999, 266 pp.
[25] A.N. Strahler, Dynamic basis of geomorphology, Geol. Soc. Am. Bull. (1963) 923–938.
[26] S.E. Lee, S.S. Byun, J.K. Oh, S.C. Lee, I.H. Chang, G. Choe, S.K. Hong, Significance of macroscopic tumor necrosis as a prognostic indicator for renal cell carcinoma, J. Urol. 176 (October (4 Pt 1)) (2006) 1332–1337 (discussion 1337–1338).